Doppler-free spectroscopy

1 Introduction

The invention of the laser in the 1960s revolutionized precision spectroscopy, making it possible to study atomic and molecular structures with unprecedented resolution and accuracy. Lasers, characterized by their narrow linewidth, tunability, and coherence, enabled the observation of fine spectral features that were previously unresolved. This advancement led to significant insights into the structure of atoms and molecules, establishing precision spectroscopy as a vibrant field of research.

Laser spectroscopy also laid the groundwork for groundbreaking advancements in laser cooling and atom trapping, culminating in the 1995 realization of Bose-Einstein condensation in alkali gases. In laboratories working with trapped atomic atoms and molecules, Doppler-free saturated absorption spectroscopy is widely employed as a key technique for locking lasers to specific atomic transitions.

2 Qualitative picture for two-level atoms

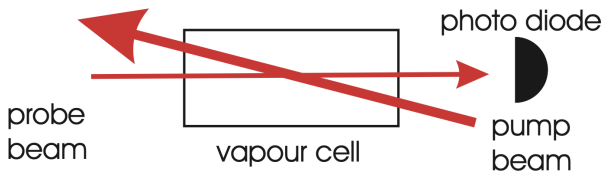

Figure 1: Basic experimental arrangement for saturation spectroscopy.

The core of the experimental setup for Doppler-free saturation spectroscopy is shown in Fig.1. Two counter-propagating laser beams, derived from a single laser source, pass through an atomic vapor cell. The pump beam, which has high intensity, bleaches the atomic gas by saturating the atomic transition, making the gas transparent at certain frequencies. Meanwhile, the transmittance of the weaker probe beam, which typically has an intensity about ten times lower, is measured using a photodiode to generate the spectroscopic signal.

Signal without the pump beam To understand the expected signals, consider a two-level atom with a ground state $|g\rangle$ and an excited state $|e\rangle$. If only the probe beam passes

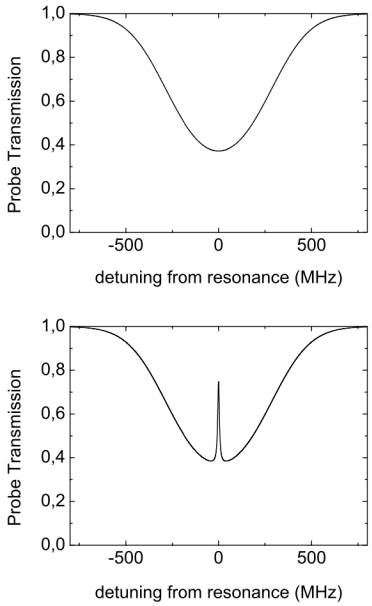

Figure 2: Transmission signal for a probe beam without (top) and with (bottom) an intense pump beam present.

through the vapor cell (with the pump beam blocked), the observed signal is a simple absorption line dominated by Doppler broadening (Fig2 top). This broadening arises because atoms in the vapor move with a range of velocities, causing the observed transition frequencies to shift according to the Doppler effect. The resulting absorption profile has a characteristic Gaussian shape. At room temperature, the Doppler width is typically two orders of magnitude larger than the natural linewidth, which is the intrinsic frequency width of the atomic transition.

Signal with the pump beam: The Lamb dip When the pump beam is added, a sharp, narrow spike—known as the Lamb dip—appears in the probe beam's transmission signal at the resonance frequency $\nu = \nu_0$ of the atomic transition (Fig2 bottom). This feature, first explained by Willis Lamb, highlights the power of saturation spectroscopy.

For the Lamb dip to occur, we need atoms with zero velocity along the axis of the vapor cell so that they can see the same frequency from both the pump and probe beams. Why? Atoms moving in one direction experience a blue-shifted pump beam and a red-shifted probe beam (or vice versa), meaning that the two beams are never resonant with the same atoms unless their velocity component along the beam axis is zero. For zero-velocity atoms, the intense pump beam excites a significant portion of the population to the excited state $|e\rangle$. These atoms absorb photons from the pump beam and decay back to the ground state $|g\rangle$ via spontaneous emission. At high pump intensities, the ground-state population is significantly depleted, reducing the absorbance of the probe beam. This results in a sharp increase in the probe beam's transmission at $\nu = \nu_0$, creating the Lamb dip. Note that at extremely high pump intensities, the atomic transition becomes saturated, meaning that approximately half of the atoms are in the ground state and half in the excited state, leading to no net absorption of the probe beam. This is why we call this method saturated absorption.

The width of the Lamb dip is significantly narrower than the Doppler width. If the laser used in the experiment has a sufficiently small intrinsic linewidth, the Lamb dip can approach the natural linewidth of the atomic transition, revealing fine details of the spectroscopic feature.

3 Quantitative picture to describe saturated spectroscopy

In the previous section we gave a qualitative picture for saturated spectroscopy. Here we want to provide a more quantitative picture.

4 Optical Depth

The intensity I of a single weak laser beam propagating through a vapor cell changes according to Beer's law:

$$\frac{dI}{dx} = -\alpha(\nu)I, \tag{1}$$

where $\alpha(\nu)$ is the frequency-dependent extinction coefficient. For a single weak beam, to a good approximation, α does not depend on the position. The overall transmission through the vapor cell of length l is given by:

$$I_{\text{out}} = I_{\text{in}} e^{-\alpha(\nu)l} = I_{\text{in}} e^{-\tau(\nu)}, \tag{2}$$

where $\tau(\nu) = \alpha(\nu)l$ is called the *optical depth*.

The contribution from a specific velocity class of atoms $(v, v + dv)$ to the optical depth $\tau(\nu)$ can be expressed as:

$$d\tau(\nu, v) = l\sigma(\nu, v)dn(v), \tag{3}$$

where $\sigma(\nu, v)$ is the absorption cross-section, and $dn(v)$ is the fraction of atoms within the velocity range $(v, v + dv)$.

Absorption Cross Section The absorption coefficient $\sigma(\nu, v)$ has a Lorentzian profile with natural linewidth Γ and a Doppler-shifted resonance frequency:

$$\sigma(\nu, v) = \sigma_0 \frac{\Gamma^2/4}{(\nu - \nu_0 + \nu_0 v/c)^2 + \Gamma^2/4}, \tag{4}$$

where σ_0 is the on-resonance absorption cross-section, ν_0 is the resonance frequency, v is the velocity of the atoms along the laser propagation direction, c is the speed of light, Γ is the natural linewidth of the atomic transition.

The value of σ_0 depends on the nature of the atomic transition (e.g., dipole or quadrupole) and the polarization of the incident light.

Fraction of atoms with velocity v The fraction of atoms $dn(v)$ belonging to a specific velocity class follows a Boltzmann distribution:

$$dn(v) = n_0 \sqrt{\frac{m}{2\pi k_B T}} e^{-mv^2/2k_B T} dv, \tag{5}$$

where n_0 is the total atomic density, m is the mass of the atom, T is the temperature, k_B is Boltzmann's constant.

The density of atoms in the vapor cell is given by $n_0 = N/V$, where N is the total number of atoms and V is the volume of the vapor cell. By combining the relevant factors, the differential contribution to the optical depth for a laser frequency ν and atomic velocity v is given by:

$$d\tau(\nu, v) = \frac{2}{\pi} \frac{\tau_0 \nu_0}{\sigma_0 \Gamma c} \sigma(\nu, v) e^{-mv^2/2k_B T} dv, \tag{6}$$

where the overall normalization is chosen such that τ_0 represents the **optical depth at resonance**. Specifically:

$$\tau_0 = \int d\tau(\nu_0, v), \tag{7}$$

with the integral carried out over all velocity classes.

4.1 Effect of a pump beam

For Doppler-free saturation spectroscopy, we must account for the effect of an additional strong pump beam. Due to the strong laser beam, a significant fraction of the atoms in the vapor cell will occupy their excited state. Since atoms can only absorb light when they are in the ground state, we must include a factor $(N_g - N_e)/N$ in Equation (6), where N_g and N_e represent the ground-state and excited-state populations, respectively.

4.2 Rate Equations

The populations of the two states evolve according to the following rate equations:

$$\dot{N}_g = \Gamma N_e - \sigma \Phi (N_g - N_e), \tag{8}$$

$$\dot{N}_e = -\Gamma N_e + \sigma \Phi (N_g - N_e), \tag{9}$$

where:

- The first term in each equation describes spontaneous emission,
- The second term describes stimulated absorption and emission.

Here, $\Phi = I/h\nu$ is the incident photon flux.

Since $N_g + N_e = N$ remains constant, we can eliminate N_g from the equations. Substituting, the physics is fully described by the equation for N_e:

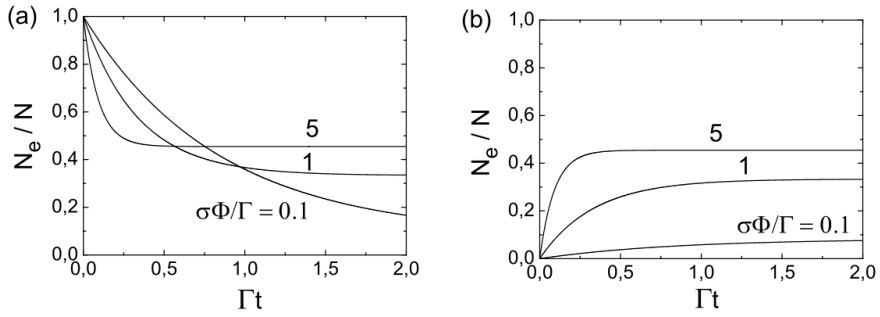

Figure 3: Excited-state population N_e as a function of time. (a) shows an exponential decay of population with $N_e(t=0) = N$, in (b) the population in N_e increases exponentially in time. In any case the population in the excited state satisfies $N_e < N/2$ for long times.

$$\dot{N}_e = -(\Gamma + 2\sigma\Phi)N_e + \sigma\Phi N. \tag{10}$$

General solution of the population Dynamics The differential equation (10) is solved as:

$$N_e(t) = \left[N_e(0) - \frac{N\sigma\Phi}{\Gamma + 2\sigma\Phi}\right] e^{-(\Gamma+2\sigma\Phi)t} + \frac{N\sigma\Phi}{\Gamma + 2\sigma\Phi}. \tag{11}$$

Several examples of this general solution are shown in Fig.3.

Case 1: no radiation field In the absence of a radiation field, the population in the excited state exhibits a purely exponential decay, given by:

$$N_e(t) = N_e(0)e^{-\Gamma t}. \tag{12}$$

Case 2: Weak pump beam When a weak light source is present, i.e., $\sigma\Phi \ll \Gamma$, and assuming that initially all atoms are in the ground state ($N_e(0) = 0$), the population in the excited state grows as:

$$N_e(t) = \frac{N\sigma\Phi}{\Gamma}\left[1 - e^{-\Gamma t}\right]. \tag{13}$$

After a characteristic time of Γ^{-1}, the population reaches a steady-state value of:

$$N_e(\infty) = \frac{N\sigma\Phi}{\Gamma} \ll N. \tag{14}$$

Case 3: Strong pump beam For typical saturation spectroscopy (and in the experimental setup we are going to build), a very strong pump laser is used, satisfying $\sigma\Phi \gg \Gamma$. In this case, the excited state population approaches a fully saturated transition:

$$N_e(t) = \left[N_e(0) - \frac{N}{2}\right] e^{-2\sigma\Phi t} + \frac{N}{2}. \tag{15}$$

As $t \to \infty$, the system reaches a saturation value of:

$$N_e(\infty) \to \frac{N}{2}. \tag{16}$$

Here, saturation implies that half of the atomic population resides in the excited state. Even with infinite power, it is not possible to exceed this limit in a two-level system.

4.3 Power Broadening in Laser Spectroscopy

A well-known phenomenon in laser spectroscopy is power broadening, which also appears in the steady-state solutions of Eq. (11). In the limit where $(\Gamma + 2\sigma\Phi)t \gg 1$, the steady-state population in the excited state is given by:

$$\frac{N_e(\infty)}{N} = \frac{\sigma\Phi}{\Gamma + 2\sigma\Phi}. \tag{17}$$

By substituting Eq. (4) and writing the frequency detuning as $\Delta\nu = (\nu - \nu_0 - \nu_0 v/c)$ (with the opposite sign due to the Doppler shift for the pump beam), we can rewrite the expression for the population as:

$$\frac{N_e(\infty)}{N} = \frac{\sigma_0\Phi\Gamma/4}{\Delta\nu^2 + \Gamma^2/4 + \sigma_0\Phi\Gamma/2}. \tag{18}$$

This equation represents a Lorentzian function whose "power-broadened" half-width depends on the incident photon flux. Specifically, the half-width at half-maximum (HWHM) is given by:

$$\Delta_{1/2} = \frac{\Gamma}{2}\left(1 + \frac{2\sigma_0\Phi}{\Gamma}\right)^{1/2}. \tag{19}$$

Introducing the **saturation parameter** $s = \Phi/\Phi_{\text{sat}}$, where $\Phi_{\text{sat}} = \Gamma/(2\sigma_0)$, we can express the population in the excited state as:

$$N_e = \frac{s/2}{1 + s + 4\Delta^2/\Gamma^2}. \tag{20}$$

This expression provides all the necessary ingredients to compute a saturated absorption spectrum for a two-level atom.

The **saturation intensity** I_{sat} can be expressed as:

$$I_{\text{sat}} = \frac{2\pi^2 hc\Gamma}{3\lambda^3}. \tag{21}$$

For the D_2 line in ^{87}Rb with a natural linewidth of $\Gamma = 6\,\text{MHz}$, the saturation intensity is approximately:

$$I_{\text{sat}} \approx 1.65\,\text{mW/cm}^2. \tag{22}$$

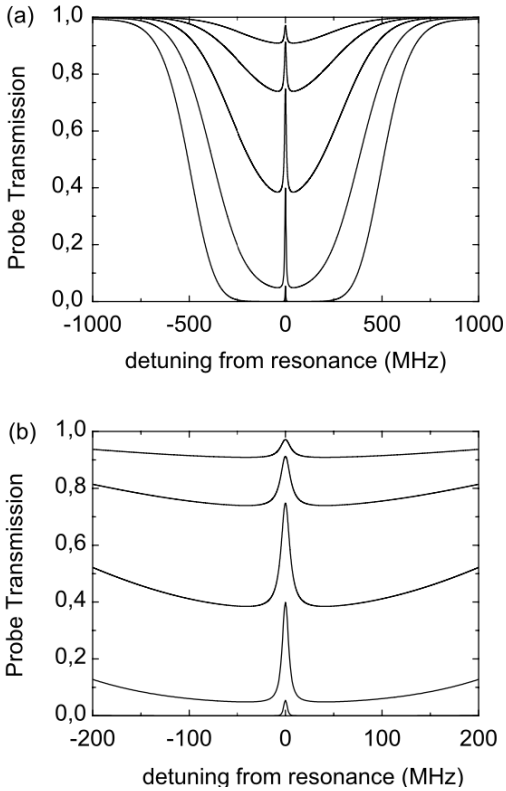

Figure 4: Probe transmission as a function of laser frequency for different vapour densities. (b) is a zoom into the region around ν_0: for very high densities the saturated-absorption peak vanishes

5 Calculated Saturated-Absorption Spectra

In the previous sections, we have seen that a saturated absorption spectrum is primarily determined by two externally adjustable parameters: the **pump intensity** and the **on-resonance optical depth**. The latter, assuming a fixed temperature and a specific atomic species, is proportional to the **vapor density** inside the cell.

Figure 4 illustrates absorption spectra for different vapor densities in the cell:

- **Low Densities:** At low atomic densities, the probe absorption is weak and exhibits a *Gaussian profile*.
- **Intermediate Densities:** As the density increases, both the absorption and the profile width increase. The profile becomes broader and deeper but retains its Gaussian shape.
- **High Densities:** At very high densities, the absorption saturates, and the profile deviates from a Gaussian shape. Even far from resonance, the probe beam is almost completely absorbed. However, *on-resonance absorption is reduced* due to the strong pump beam, resulting in the appearance of the **saturated absorption feature** (e.g., the Lamb dip). For increasing densities, this feature becomes smaller and less pronounced (see Fig. 4b).

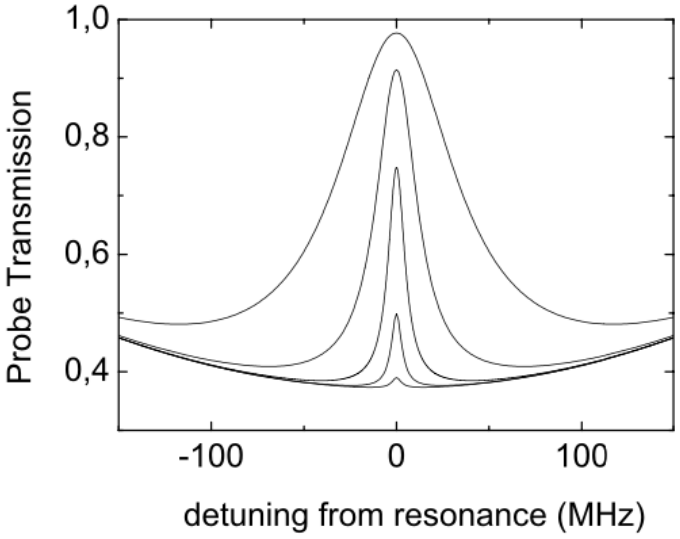

Figure 5: Saturated-absorption peak for fixed vapour density and varying pump beam intensity. The effect of power broadening is clearly visible.

Effectively, increasing atomic density corresponds to an increase in the absolute number of atoms in the ground state, which leads to greater absorption at $\nu = \nu_0$ (on resonance).

Next, consider the effect of varying the pump beam intensity while holding the atomic density fixed, as shown in Figure 5:

- **Increasing Pump Intensity:** Higher pump intensities enhance the saturation effect, increasing both the height and width of the **Lamb dip**. This behavior reflects the *power broadening* of the atomic transition.

Increasing the pump beam intensity causes stronger saturation and power broadening of the absorption profile (Fig.5).

6 Multi-level atoms - Rubidium

Alkali atoms are the workhorse in many of today's experiments involving the trapping, cooling, and manipulation of atoms. Their popularity stems from several key advantages:

- **Simple Level Structure:** Alkali atoms have a relatively simple, hydrogen-like level structure due to the presence of a single valence electron in the outer shell. This makes them particularly suitable for precision experiments and theoretical modeling.
- **Accessible Transition Frequencies:** Unlike hydrogen, alkali atoms have transition frequencies from the ground to the first excited state that typically lie in the visible or near-infrared part of the spectrum. These wavelengths are easily accessible using relatively inexpensive and reliable commercially available lasers.

In this experiment, rubidium is used as the atomic species. Rubidium offers a transition frequency at 780 nm, which is well within the range of standard diode lasers. This wavelength can be conveniently generated by widely available and robust laser systems, making rubidium an ideal choice for experiments requiring optical manipulation.

6.1 Fine-Structure Splitting

In the case of rubidium, the inner four electronic shells are filled, and only the single outer (5s) valence electron determines the angular momentum configuration of the atom. The state of the electron is completely described by its orbital angular momentum $\vec{L}$ and its spin $\vec{S}$. These two angular momenta couple in the usual way to form the total angular momentum J of the electron. Hence, J can take the values $|L - S| \leq J \leq |L + S|$.

The coupling is driven by the so-called spin-orbit interaction, which can be written as:

$$V_{\text{so}} = A_{\text{fs}} \, \vec{L} \cdot \vec{S}$$

This is a relativistic effect and can be derived from the Dirac equation for spin-$\frac{1}{2}$ particles. In simple terms, the spin-orbit coupling represents the magnetic interaction energy of the electron's spin in the magnetic field created by the relative motion of the nucleus and the electron. For a detailed discussion, refer to any good book on (relativistic) quantum mechanics.

The spin-orbit coupling results in what is known as **fine-structure splitting** for different values of the total angular momentum $\vec{J}$.

For alkali atoms, the electronic states are fully specified using the Russell-Saunders notation $n^{(2S+1)}L_J$, where n denotes the principal electronic quantum number. For rubidium (Rb), $n = 5$, and the ground state is denoted as $5^2S_{1/2}$. The fine-structure splitting between the first excited states $5^2P_{1/2}$ and $5^2P_{3/2}$ is 7123 GHz.

6.2 Hyperfine splitting

If the rubidium nucleus carried no spin, the $5^2S_{1/2}$, $5^2P_{1/2}$, and $5^2P_{3/2}$ energy levels would be singlets with no external fields applied. However, this is not the case; there are two natural isotopes of rubidium: ^{87}Rb with a nuclear spin $I = \frac{3}{2}$ and ^{85}Rb with $I = \frac{5}{2}$, with ^{85}Rb having a higher abundance of 72%.

The non-vanishing nuclear spins have magnetic and (electric) quadrupolar moments associated with them, leading to the so-called **hyperfine splitting** of the atomic energy levels.

The first contribution to the hyperfine splitting is the energy of the nuclear magnetic (dipole) moment $\vec{\mu}_{\text{nucl}}$ in the magnetic field $\vec{B}_{\text{el}}$ generated by the valence electron at the position of the nucleus. This interaction can be expressed as:

$$H_{\text{hf}} = -\vec{\mu}_{\text{nucl}} \cdot \vec{B}_{\text{el}} \quad (19)$$

Since $\vec{\mu}_{\text{nucl}}$ is proportional to the nuclear spin $\vec{I}$, and $\vec{B}_{\text{el}}$ is proportional to the total angular momentum of the valence electron $\vec{J}$, the Hamiltonian can be rewritten as $\alpha \vec{I} \cdot \vec{J}$. The parameter α is called the magnetic hyperfine structure constant and has units of energy, that is $\vec{I}$ and $\vec{J}$ are taken to be dimensionless.

The second contribution to the hyperfine splitting arises from the electrostatic interaction between the valence electron and the non-vanishing electric quadrupole moment of the nucleus. This interaction can be expressed in terms of the nuclear and electron angular momenta $\vec{I}$ and $\vec{J}$ as follows:

$$H^{hf}_{\text{quadr}} = \frac{\beta}{2I(2I-1)J(2J-1)}\left[3(\vec{I}\vec{J})^2 + \frac{3}{2}(\vec{I}\vec{J}) - I(I+1)J(J+1)\right], \tag{23}$$

where, in analogy to the magnetic case, β is called the electric quadrupole interaction constant and has units of energy.

These two interactions lead to a coupling of the nuclear angular momentum $\vec{I}$ and the electron angular momentum $\vec{J}$ to the total angular momentum $\vec{F} = \vec{I} + \vec{J}$, where F can take any value between $|J - I|$ and $J + I$. Associated with this coupling is a splitting into hyperfine levels, which are labeled by the hyperfine quantum number F. Electric dipole transitions between hyperfine levels must obey the selection rules:

$$\Delta L = \pm 1 \quad (21)$$

$$\Delta F = 0, \pm 1 \quad \text{(but not } 0 \to 0) \quad (22)$$

$$\Delta J = 0, \pm 1 \quad (23)$$

Using the definition for $\vec{F}$ and forming $\vec{F} \cdot \vec{F}$, it is possible to write:

$$\vec{I} \cdot \vec{J} = \frac{F(F+1) - J(J+1) - I(I+1)}{2} =: \frac{C}{2}$$

Hence, for given J and I, the frequencies ν_F of the various hyperfine levels are given by:

$$\nu_F = \nu_J + \frac{AC}{2} + B\left[\frac{3C(C+1) - 4I(I+1)J(J+1)}{8I(2I-1)J(2J-1)}\right], \tag{24}$$

where ν_J is the frequency (energy) of the state $n(2S+1)L_J$ without the hyperfine interaction. In the above expression, $A = \frac{\alpha}{\hbar}$ and $B = \frac{\beta}{\hbar}$ have units of Hz.

It turns out that for the $5^2S_{1/2}$ ground state of both ^{85}Rb and ^{87}Rb, the last term in Eq. (24) is zero. Therefore, the hyperfine splitting in the ground state is characterized by a single parameter $A(5^2S_{1/2})$, which for ^{87}Rb is $A(5^2S_{1/2}) = 3417.34\,\text{MHz}$ and for ^{85}Rb is $A(5^2S_{1/2}) = 1011.91\,\text{MHz}$.

In contrast, for the first excited states $5^2P_{1/2}$ and $5^2P_{3/2}$, the hyperfine parameters A and B are both different from zero and are typically on the order of a few tens of MHz, which is much smaller than for the ground state.

Energy level diagrams of the states $5^2S_{1/2}$, $5^2P_{1/2}$, and $5^2P_{3/2}$ for both ^{85}Rb and ^{87}Rb are shown in Fig.6.

It is the main goal of this experiment to measure the hyperfine constants A and B for the state $5^2P_{3/2}$ of the two isotopes of rubidium.

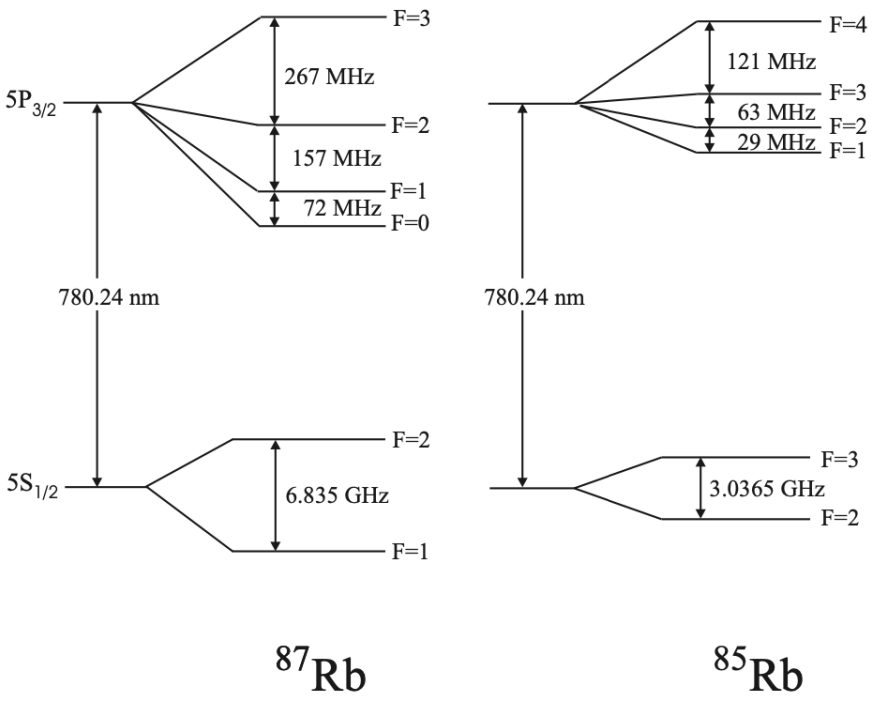

Figure 6: Level scheme for the $5S_{1/2} \leftrightarrow 5P_{3/2}$ transition in $^{8}5$Rb and $^{8}7$Rb.